Asian Journal of Chemistry; Vol. 35, No. 9 (2023), 2069-2077

ASIAN JOURNAL OF CHEMISTRY

https://doi.org/10.14233/ajchem.2023.28041

Effect of ZnO on the Structural and Magnetodielectric Properties of $MgFe_2O_4$ Nanocomposite Prepared by Sol-Gel Method

T. VEERAMANI[1], C. VENKATARAJU[1,*], V. PORKALAI[1] and R. SAGAYARAJ[2,*]

[1]P.G. & Research Department of Physics, Thiru.Vi.Ka. Government Arts and Science (Affiliated to Bharathidasan University), Thiruvarur-610003, India
[2]P.G. & Research Department of Physics, St. Joseph's College of Arts and Science (Autonomous) (Affiliated to Annamalai University), Cuddalore-607001, India

*Corresponding authors: E-mail: tvkphymani@gmail.com; sagayarajnancy@gmail.com

Received: 19 May 2023; *Accepted*: 15 June 2023; *Published online*: 31 August 2023; AJC-21345

Zinc oxide doped magnesium ferrite ($Mg_{1-x}Zn_xFe_2O_4$) nanocomposite was synthesized using sol-gel method and demonstrated to have a cubic spinel structure, with a range of crystallite sizes (19-40 nm) and lattice constants (8.432-8.399 Å). The material was found to have two prominent vibrational modes for tetrahedral (446 cm^{-1}) and octahedral (584 cm^{-1}). The dielectric constant was higher at low frequencies and decreased at higher frequencies, while the saturation magnetization decreased (16 to 6 emu/g) gradually with an increase in Zn^{2+}, likely due to the presence of non-magnetic Zn^{2+}. The magneto-dielectric constant was found to increase with the magnetic field for $MgFe_2O_4$ and up to a magnetic field of 2000 Oe for the zinc magnesium nanocomposites, after which it decreased for higher magnetic fields. A positive and negative change in magneto-capacitance as a function of the magnetic field was also observed. The antibacterial activity suggests that the substitution of Zn^{2+} into magnesium ferrite can be an effective method for improving antibacterial activity, with the potential to damage the bacterial membrane and other components through positively charged ions and ROS generated by nanoparticles. Potential uses for this synthetic material include magneto-optical recording and magnetic biosensors.

Keywords: Zinc oxide, Magnesium ferrite, Sol-Gel method, Dielectric constant, Magneto dielectric, Coercivity, Ferrimagnetic.

INTRODUCTION

Ferrite is an iron or other divalent cations component that is made up of one or more ferromagnetic materials, often either metal alloys or ceramic compounds. The general formula for ferrites is $A^{2+}B_2^{3+}O_4$, for example $Fe^{2+}Fe_2^{3+}O_4$, which is representative of its iron oxide content. The most common type of ferrite is magnetic, which is composed of iron and an oxide, such as chromium oxide or manganese oxide [1]. Ferrite magnets typically have a weak magnetic field, but they are able to store energy in their magnetic domains, making them ideal for applications like power transformers. Iron ferrite is a type of ferrite material composed of iron and one or more ferromagnetic materials, such as metal alloys or ceramic compounds [1,2].

Zinc ferrite is an artificial magnetic material composed of zinc oxide and iron oxide. It has a spinel structure, which consists of an ordered arrangement of cations and anions, such as Zn^{2+} and Fe^{3+} in this case. This structure results in a strong magnetic field and makes zinc ferrite an ideal choice for applications such as data storage and magnetic recording [3]. Magnesium ferrite is a ferromagnetic compound of magnesium oxide and iron oxide. This material has a spinel structure formed by an ordered arrangement of cations and anions, specifically Mg^{2+} and Fe^{3+}. The resulting strong magnetic field is advantageous for uses like high frequency amplifiers and radio antennas [4]. Spinel structures are composed of oxygen and metal cations, arranged in a cubic lattice. There are three main types of spinel structures such as normal spinel, inverse spinel and mixed spinel. The cation and anion sites within the lattice are distributed in an ordered fashion is called normal spinel, such as in magnesium ferrite ($MgFe_2O_4$). The cation and anion sites within the lattice are distributed in an inverted fashion is said to be inverse spinel, such as in magnetite (Fe_3O_4). Zinc-doped magnesium ferrite is a magnetic material composed of cobalt oxide, zinc oxide and iron oxide. It has a disordered spinel structure, which consists

of a random arrangement of cations and anions such as Co^{2+} and Mg^{2+} and zinc doped cobalt ($Co_{1-x}Zn_xFe_2O_4$) ferrite spinel [5].

The normal spinel structure of $MgFe_2O_4$ ferrite prepared by electrospinning is consistent with divalent Mg^{2+} cations occupying all the A sites and trivalent Fe^{3+} cations occupying all the B sites. This means that the charge neutrality requirement is satisfied by having both positive and negative ions in the crystal lattice. All the anions in the lattice, either oxygen or any counter ions, adjust their charges to bring the overall charge of the unit cell to zero [6]. The magnetic characterization of $MgFe_2O_4$ ferrite reveals that Zn doping changes the spin states of Fe^{3+} and this in turn affects its interaction with other ions. The super-exchange interaction between the Fe^{3+} ions and the O^{2-} anions leads to an increase in magnetization and a decrease in the Curie temperature. This means that the material's magnetism is enhanced at lower temperatures. The lattice parameter decreases with increasing Mg content, thus obeying Vegard's law. The ionic radius of Mg^{2+} ion (0.65 Å) is smaller than that of Zn^{2+}ion (0.83 Å) and thus causes an effective decrease in the lattice constant [7]. Zhang *et al.* [8] examines the exchange interactions between two sub-lattices of $MgFe_2O_4$ ferrites. It was found that the antiferromagnetic A-B interaction is stronger than the ferromagnetic B-B and A-A interactions, while the ferromagnetic A-A interaction is the weakest. Furthermore, the non-magnetic Mg^{2+} ions occupy the tetrahedral A sites and the magnetic Fe^{3+} ions occupy the octahedral B sites. Zn-doped $MgFe_2O_4$ ferrites were also studied, in which Zn^{2+}ions preferentially substitute for Fe^{3+}ions, thus increasing the valence surrounding trivalent Fe^{3+} ions and Fe^{3+} ions contributes to an increase in saturation magnetization. The results of this study provide a better understanding of the exchange interactions between two sub-lattices of $MgFe_2O_4$ ferrites and how Zn-doping can affect their magnetic properties.

This study investigates the influence of Zn-substitution on the inverse spinel structure of Mg-ferrite. It is proposed that a controlled Zn-substitution could alter the structure from an inverse to a normal spinel *via* a mixed structure, thus leading to systematic changes in the cationic distribution between A and B sites. This would consequently have a notable effect on the magnetic properties of the ferrite. It is also observed that any deviation from the ideal inverse or normal spinel structure may even lead to non-equilibrium site occupancy, which is commonly observed in nano-structured ferrites [9-11]. Liu *et al*. [12] investigated the effect of Zn-substitution on the magnetization of Mg-ferrite samples. It is found that three types of exchange interactions exist between the unpaired electrons of two ions lying in A- and B-sites. The Fe^{3+} ions tend to occupy B-sites, while Zn^{2+} ions are non-magnetic and prefer to occupy A-sites. The substitution of Zn^{2+} into the lattice leads to increased Fe^{3+} ions on B-sites, resulting in an increase in magnetization of B-sites and a decrease in magnetization of A-site. It was also found that Zn^{2+} ions show a strong preference for the tetrahedral interstitial sites (A-sites) and can replace both Mg^{2+} and Fe^{3+} ions located in these sites. The substitution leads to an increase in the number of Fe^{3+} ions on the B-sites, resulting in an increase in overall magnetization of the lattice.

Magnetic moment of $Mg_{1-x}Zn_xFe_2O_4$ sample depends on the migration of Fe^{3+} (5 μB) ions between A and Bsite as Zn^{2+} (0 μB) and Mg^{2+} (0 μB) ions are diamagnetic in nature [13,14]. In present investigation, we have studied ZnO embedded in the $MgFe_2O_4$ matrix. The phase of zinc-doped magnesium ferrite is a ferrimagnetic material, meaning it exhibits a magnetic field when exposed to an external magnetizing force. This material has a spinel structure, which consists of a random arrangement of cations and anions, such as Zn^{2+} and Mg^{2+} in this case. The aim of this work is to investigate the properties of zinc-doped magnesium ferrite for potential biomedical and technological applications. X-ray diffraction (XRD), Fourier transform infrared spectroscopy (FTIR), field emission scanning electron microscopy (FE-SEM), dielectric constant, magneto-dielectric constant and vibrating sample magnetometer (VSM) measurements were conducted in order to determine the properties of the material. The results provide insight into the possible biomedical and technological applications of Zn-doped $MgFe_2O_4$ as a multifunctional material. This work also discusses the structural, magnetic and dielectric properties of the material, with particular focus on the impact of Zn-substitution on the spinel structure. It was observed that Zn^{2+}ions prefer to occupy the tetrahedral A-sites, while Fe^{3+} ions tend to occupy the octahedral B-sites. The substitution leads to increased Fe^{3+} ions on B-sites, resulting in an increase in magnetization of the B-sites and a decrease in magnetization of A-site. Furthermore, the magneto-dielectric constant of the composite material was found to be positive up to 2000 Oe before decreasing for higher magnetic field strengths. These findings provide important information about the properties of Zn-doped magnesium ferrite and will help researchers gain insight into its potential applications in the biomedical and technological fields.

EXPERIMENTAL

Sol-gel method: Nanoparticles of $Mg_{1-x}Zn_xFe_2O_4$ were prepared using the sol-gel method. The precursor solutions of $Mg(NO_3)_3{\cdot}6H_2O$, $Zn(NO_3)_3{\cdot}6H_2O$ and $Fe(NO_3)_3{\cdot}9H_2O$ were mixed with ethylene glycol and stirred until homogeneous. This solution was then stirred well to 80 ºC for 4 h by magnetic stirrer. To achieve this synthesis, ethylene glycol was added to maintain a pH of 11 in order to obtain a white precipitate, which was washed with distilled water several times. The nanocomposites were then dried at 100 ºC and calcined at 600 ºC for 4 h. The structure and crystallite size was determined by a PAN analytical X-ray diffractometer (XRD) using Cu*K*α radiation (λ = 1.54 Å). Data were collected every 0.02º in the angle range 20º-70º in 2θ. The scanning electron microscope (SEM) imaging was carried out using the CAREL ZEISS model: EVO18 equipment for the surface morphology analysis. The magnetic measurement was performed using a vibration sample magnetometer (VSM quantum design) at room temperature. The dielectric properties were measured using HIOKI 3532-50 LCR HI TESTER equipment in the frequency range of 100 Hz to 1 MHz. The magneto-dielectric measurement for the samples was recorded at room temperature using an electromagnet under a varying magnetic field up to 0.8 T.

Preparation of medium: Nutrient agar medium was used to culture bacteria and other microorganisms and consists of 28 g of nutrient agar suspended in 1000 mL of distilled water. The mixture must then be heated to boiling and completely dissolved before being sterilized by autoclaving at 15 lbs pressure (121 ºC) for 15 min. After the medium has been sterilized, it can be poured into sterile Petri plates for use in experiments.

Microorganisms: Two types of bacteria were used in a biological assay: *Staphylococcus aureus* (MTCC 3160) and *Escherichia coli* (MTCC 732), obtained from the microbial type culture collection (MTCC) at the Institute of Microbial Technology (IMTECH) in Chandigarh, India.

Preparation of 24 h pure culture: The procedure involves suspending a loop full of microorganisms in 10 mL of physiological saline in a Roux bottle, then streaking them on appropriate culture slants and incubating them at specific temperatures (37 ºC for 24 h and 25 ºC for 48 h). Once growth is observed, the tubes are kept in 2-8 ºC until they can be used.

Preparation of samples solutions: The samples were prepared in 10, 20 and 40 µg/mL concentrations in water, while the standard solution was chloramphenicol in 25 mg/mL distilled water. The samples and standards were kept refrigerated until use for the experiment.

Disc diffusion method: Antibiogram was done by disc diffusion method using samples. Petri plates were prepared by pouring 30 mL of Nutrient agar medium. The test organism was inoculated on solidified agar plate with the help of micropipette and spread and allowed to dry for 10 min. The surfaces of media were inoculated with bacteria from a broth culture. A sterile cotton swab was dipped into a standardized microbes test suspension and used to evenly inoculate the entire surface of the Nutrient agar plates. Briefly, inoculums containing of microbial strains were spread on Nutrient agar plates. Using sterile forceps, the sterile filter papers (6 mm diameter) containing discs were loaded with 10, 20 and 40 µg/mL of each sample while 30 µL standard and 30 µL control solution were laid down on the surface of inoculated agar plate. The plates were incubated at 37 ºC for 24 h for the bacteria.

RESULTS AND DISCUSSION

XRD studies: Fig. 1 shows the XRD pattern of synthesized ZnO and $Mg_{1-x}Zn_xFe_2O_4$ nanocomposites. The XRD spectra of pure $MgFe_2O_4$ show the presence of characteristics peaks at 30.0º, 35.4º, 43.0º, 53.4º, 57.0º, 62.5º corresponding to planes (220), (311), (400), (511) and (440), respectively. All peaks indexed with help of JCPDS #73-2410 and ZnO (JCPDS # 79-0208). All peaks revealed the homogeneous cubic spinel structure. The prominent diffraction peaks indicates the formation of spinel structure and confirmed ferrite signature. The average crystallitesize and lattice constant for pure and doped samples was calculated by (311) peak using the Scherrer's formula [15]:

$$\text{Crystallite size (D)} = \frac{0.9\lambda}{\beta\cos\theta} \quad \text{(nm)}$$

where, β is the FWHM in radiation; θ is the peak position; λ is the wavelength of X-ray, for *d*-spacing values and the respective

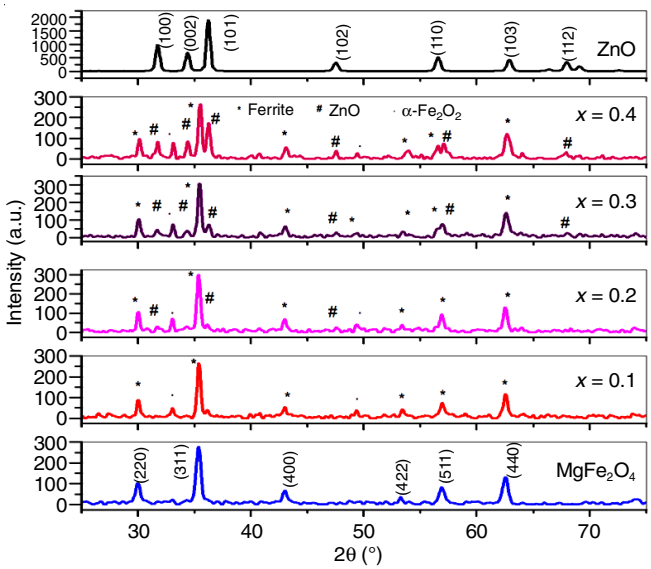

Fig. 1. XRD pattern of $MgFe_2O_4$, $Mg_{1-x}Zn_xFe_2O_4$ nanocomposites (x = 0.1, 0.2, 0.3 and 0.4)

(*hkl*) parameters obtained from the powder XRD pattern and calculated lattice constant. Pure zinc oxide has a hexagonal wurtzite structure. The lattice parameters "a" and "c" can be calculated by using the formula:

$$\frac{1}{d^2} = \frac{4}{3}\left(\frac{h^2 + k^2 + l^2}{\alpha^2} + \frac{l^2}{c^2}\right)$$

The crystallite size and lattice constant values are summarized in Table-1. It is observed that the crystallite size is decreased from 40 nm to 19 nm and 8.432 Å to 8.399 Å, respectively when Zn^{2+} is added to the $MgFe_2O_4$ ferrite matrix (Table-1). The crystallite size and lattice constant found in the $MgFe_2O_4$ ferrite matrix decreased when Zn^{2+} is added. Increased solubility of Zn^{2+} compared to other metal ions in the matrix caused the crystallite size to decrease, as Zn^{2+} has a higher charge density than other metal ions and thus can dissolve more easily. In addition, the stronger electrostatic interactions between Zn^{2+} and the framework ions enhanced the rate of nucleation and growth which further contributed to the decrease in crystallite size. The increased repulsive forces between metal ions, due to the higher charge density of Zn^{2+} and the smaller atomic radius of Zn^{2+} have resulted in shorter bond lengths and thus a decrease in lattice constant [1-3,6-8].

FTIR studies: Fig. 2 illustrates the FTIR spectra of ZnO and $Mg_{1-x}Zn_xFe_2O_4$ nanocomposites (x = 0.0, 0.1, 0.2, 0.3 and

TABLE-1
STRUCTURAL PARAMETERS DATA OF $Mg_{1-x}Zn_xFe_2O_4$

Sample	Crystallite size (nm)	Lattice constant (Ferrite phase) (Å)	Lattice constant (ZnO phase)		c/a
			a	c	
x = 0.0	40	8.432	–	–	–
x = 0.1	49	8.429	–	–	–
x = 0.2	42	8.419	3.256	5.216	1.602
x = 0.3	35	8.412	3.254	5.215	1.602
x = 0.4	19	8.399	3.253	5.212	1.602
ZnO	21	–	3.250	5.210	1.602

0.4). FTIR analysis of $MgFe_2O_4$ ferrite samples with varying Zn^{2+} substitution revealed two strong absorption bands. The shorter length band ($\Delta\nu_1$) was attributed to the stretching vibration mode of Fe^{3+}–O^{2-} in the tetrahedral (446 cm^{-1}) sub-lattice, while the longer length band ($\Delta\nu_2$) was assigned to the metal–oxygen vibration mode from Fe^{3+}–O^{2-} in the octahedral (584 cm^{-1}) sub-lattice [10,13]. With increased Zn content, the tetrahedral band shifted towards lower frequencies due to the migration of Fe^{3+} ions from the tetrahedral sites to the octahedral sites, weakening the cation-oxygen bonds in the tetrahedral sites and strengthening the Fe^{3+}–O^{2-} bond in the octahedral positions. This shift was accompanied by a slight increase in octahedral band positions. In addition to these vibrations, bands near 3440 to 1504 cm^{-1} were observed due to the H-O stretching and bending vibration modes of free or absorbed water. Another band observed in the range 1654-1636 cm^{-1} is ascribed to the bending mode vibrations of water molecules [13].

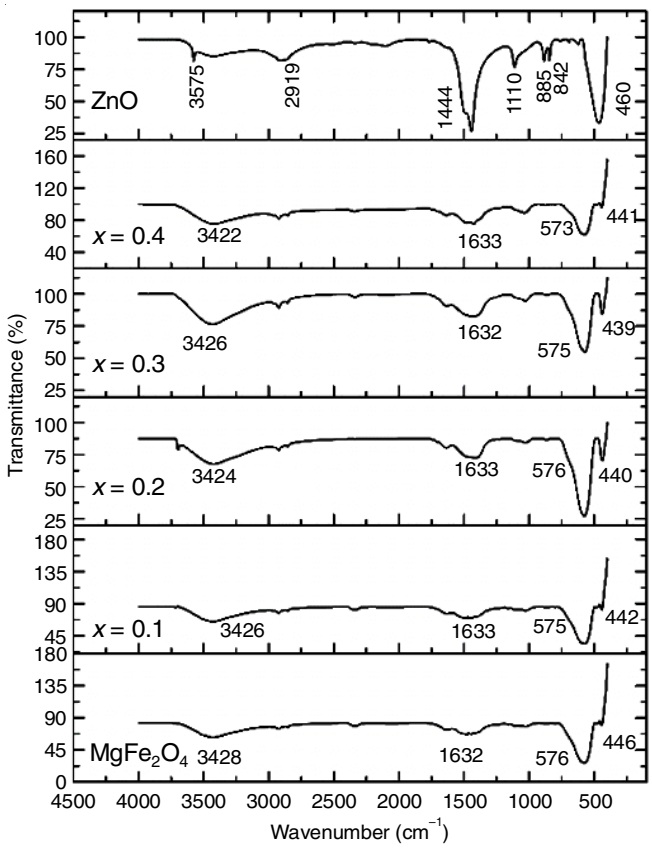

Fig. 2. FTIR spectra of $MgFe_2O_4$, $Mg_{1-x}Zn_xFe_2O_4$ nanocomposites (x = 0.1, 0.2, 0.3 and 0.4)

FE-SEM studies: Fig. 3 shows the FE-SEM image of $Mg_{0.6}Zn_{0.4}Fe_2O_4$ composite and composed of zinc, magnesium and iron, with a uniform particle size. It is produced using a coprecipitation method that involves the substitution of magnesium and zinc ions into the iron oxide crystal structure. The resulting nanoparticles have polyhedral shapes due to their tetrahedral and octahedral crystal structures, which allow them to demonstrate a good macro-structural morphology and strong ferrimagnetic properties. The particle sizes of the resulting nanoparticles obtained in order to 200 nm, making them suitable for various applications such as magnetic recording media and magnetic resonance imaging [16,17]. The polyhedral morphology of the nanoparticles is due to the stacking effect of their crystal structures, which can also contribute to their strong ferrimagnetic properties [18]. Additionally, the different metal ions in the nanoparticles can interact with each other in order to further enhance their magnetic properties. This interaction between the metal ions is known as exchange coupling and is one of the key factors determining the ferrimagnetic properties of the nanoparticle. The exchange coupling increases with the amount of substitution, which leads to an increase in the saturation magnetization and coercivity of the material [19,20]. Exchange coupling also leads to improved magnetic stability and better thermal stability, making the particle suitable for use in applications requiring higher temperatures. The results from the energy dispersive X-ray technique (EDAX) show that the precursors used in the synthesis have reacted chemically to form a single phase nanocrystalline composite of $Mg_{0.6}Zn_{0.4}Fe_2O_4$.

Dielectric studies: The dielectric constant for $Mg_{1-x}Zn_xFe_2O_4$ nanocomposites with x = 0.0, 0.2 and 0.4 varies with frequency and is shown in Fig. 4. The variation of dielectric constant with frequency is generally greater at low frequencies and less with increasing frequency. This is due to the space charge polari-

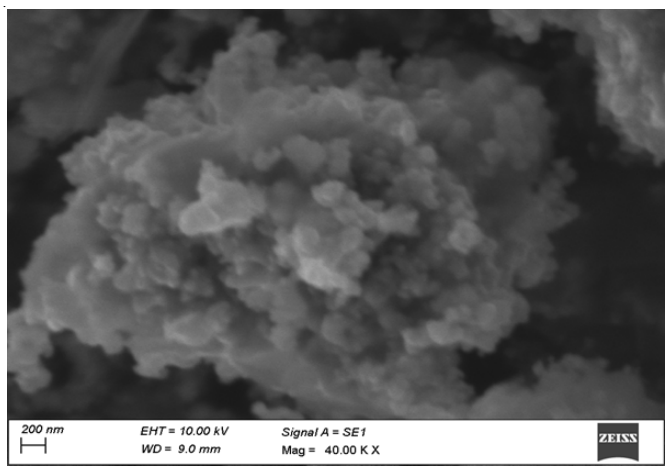

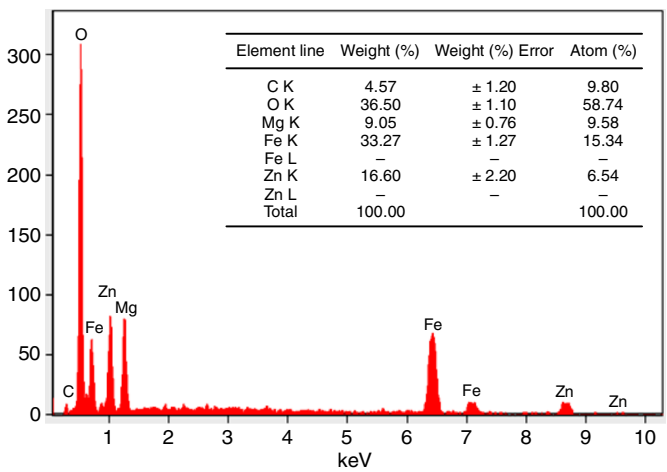

Fig. 3. FE-SEM image of $Mg_{0.6}Zn_{0.4}Fe_2O_4$ composite

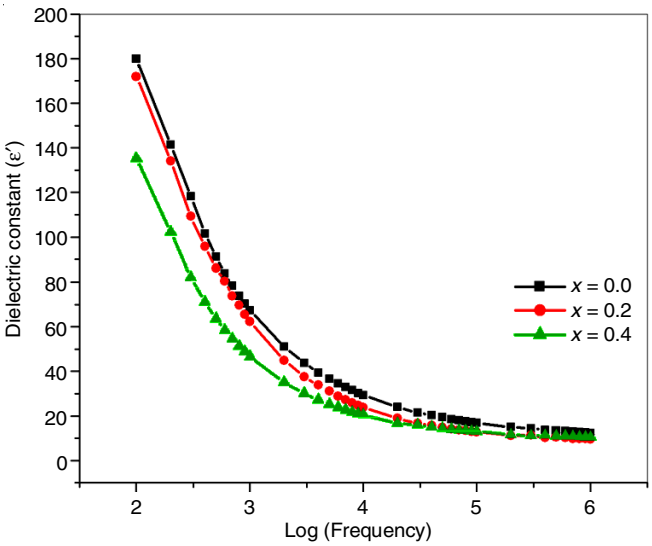

Fig. 4. Variation of dielectric constant with frequency for $Mg_{1-x}Zn_xFe_2O_4$ nanocomposites

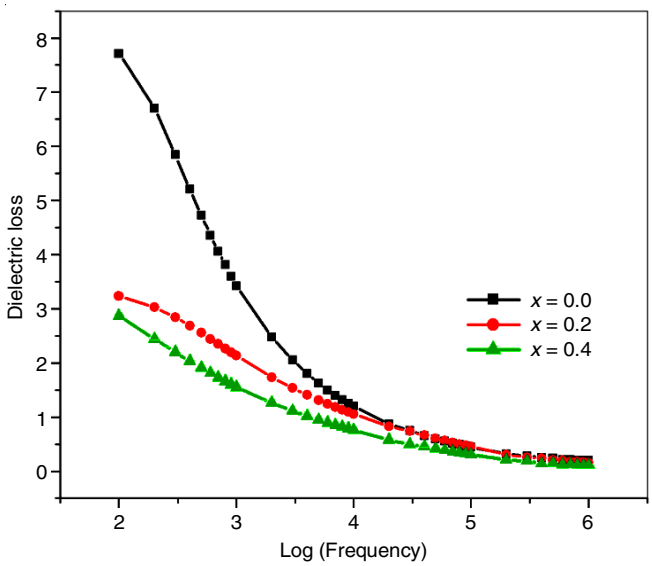

Fig. 5. Variation of dielectric loss with frequency for $Mg_{1-x}Zn_xFe_2O_4$ nanocomposites

zation model of the Maxwell–Wagner theory, which states that at low frequencies, electrons tend to accumulate at grain boundaries due to grain boundary resistance, leading to an increase in polarization. As the frequency increases, this effect decreases, resulting in a decrease in the overall dielectric constant of the system. In addition, increasing the Zn^{2+} content of nanocomposite also leads to a decrease in the dielectric constant. A dielectric relaxation peak around 150 Hz results from the Maxwell-Wagner interfacial polarization. Finally, dielectric loss decreases with increasing frequency for all the samples [21-23]. Dielectric constant of pure $MgFe_2O_4$ is 73 at 1 kHz. But as the Zn^{2+} content increases, the overall effective value of the dielectric constant of the alloy decreases. The dielectric loss for $Mg_{1-x}Zn_xFe_2O_4$ nanocomposites varies with frequency and is shown in Fig. 5. Dielectric loss factor (tan δ) shows a peak behaviour for all samples, *i.e.* initially increases before decreasing. The dielectric loss factor increases with frequency before decreasing as a result of Maxwell-Wagner interfacial polarization. The peak in dielectric loss at low frequencies may be due to the tendency of electrons to accumulate at grain boundaries due to grain boundary resistance, which increases polarization and thus dielectric loss. As the frequency increases, this effect decreases, leading to a decrease in dielectric loss. The variation of the dielectric constant and loss factor at different temperatures, as well as the effect of varying Zn^{2+} content on the dielectric constant, can provide additional insight into the behaviour of the system. Furthermore, understanding the role of grain boundaries in affecting the dielectric properties of the nanocomposite can better control the desired properties [24]. It is also useful to consider the various processes affecting the dielectric constants and loss factors of the $Mg_{1-x}Zn_xFe_2O_4$ nanocomposite. Investigating the effects of varying parameters such as grain boundary resistance, Zn^{2+} ion concentration and temperature on the dielectric constant and loss factor of the $Mg_{1-x}Zn_xFe_2O_4$ nanocomposite will provide further insight into the behaviour of the system and allow better control of its desired properties. The findings from the variation of dielectric constant with frequency curve for $Mg_{1-x}Zn_xFe_2O_4$ nanocomposite indicate that the dielectric constant is highest at lower frequencies and gets reduced at higher frequencies. This could be attributed to the lower dielectric constant of Zn^{2+} in the composite material.

Magneto-dielectric studies: Fig. 6a shows the magneto-dielectric constant for the sample $MgFe_2O_4$ measured at the different magnetic fields at room temperature. It was observed that the dielectric constant increased with an increase in the magnetic field. The magneto-dielectric effect in ferrites can be explained on the basis of magneto-resistance (MR) mechanism [1,25]. The grain boundary plays an important role as a scattering center in the spin-polarized MR effect. When a magnetic field applied, the spin alignment decreases the scattering of charges at the grain boundary and promotes the exchange of charge between Fe^{2+} and Fe^{3+} ions in the ferrite grains. This hopping of charge between Fe^{2+} and Fe^{3+}enhances the interfacial polarization and hence the dielectric constant increases [4,5,26]. Fig. 6b-e shows the variation of dielectric constant with magnetic field for the nanocomposites $Mg_{1-x}Zn_xFe_2O_4$ (x = 0.2 and 0.4). The dielectric constant increases initially with the increase in the magneticfield up to a value of 2000 Oe. Above a magnetic field of 2000 Oe, the dielectric constant decreased with the magnetic field. Fig. 7 shows the magneto-capacitance for the nanocomposites $Mg_{1-x}Zn_xFe_2O_4$ (x = 0.2 and 0.4) at room temperature with the magnetic field variation from 0 to 8 KOe at frequency 1 KHz. These measurements have been carried out to understand the relation between the magnetic and electric phases. This can be done indirectly by measuring the change in the dielectric constant as a function of an applied magnetic field [6,7,27,28]. The occurrence of magneto-dielectric/magneto-capacitance effects in the composite materials is due to several reasons such as the magnetostriction effect, magneto resistance, or magneto-electric coupling. Hence, the application of magnetic field not only affects the magnetic order but also changes the dielectric constant [28,29]. The magneto coupling (MC) can be estimated by the following relation [29]:

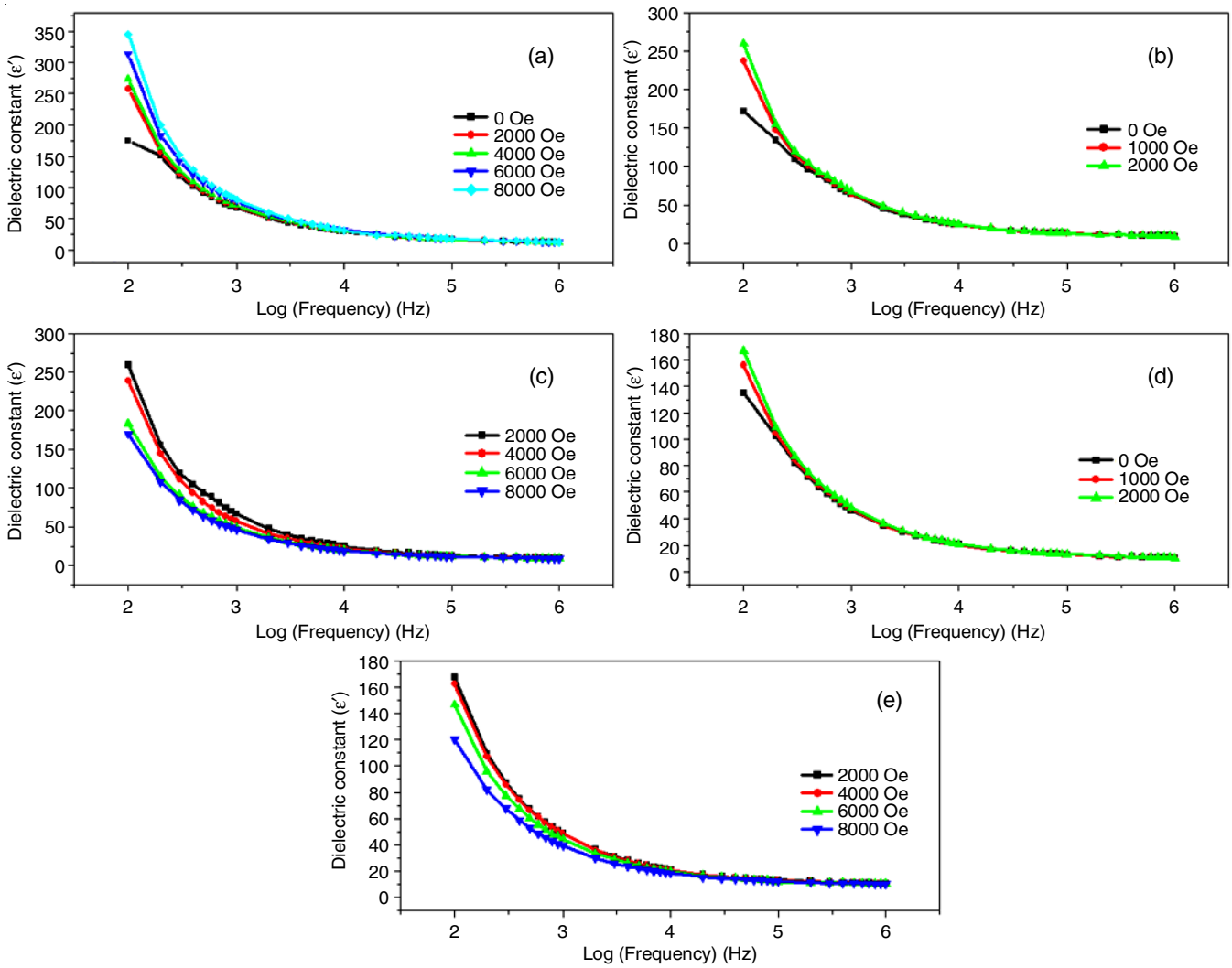

Fig. 6. Variation of dielectric constant as a function of magnetic field for the $Mg_{1-x}Zn_xFe_2O_4$ nanocomposites, (a) x = 0.0 & (b) x = 0.1 and field varying from 0 to 2000 Oe, (c) x = 0.2 and field varying from 2000to 8000 Oe, (d) x = 0.3 and field varying from 0 to 2000 Oe, (e) x = 0.4 and field varying from 2000 to 8000 Oe

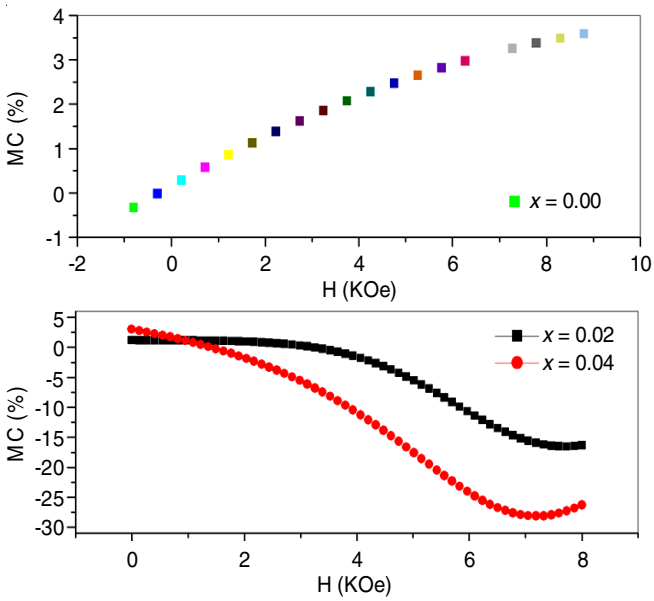

Fig. 7. Variation of magneto capacitance as a function of magnetic field for $Mg_{1-x}Zn_xFe_2O_4$, x = 0.0, 0.2, 0.4

$$MC = \frac{\varepsilon'[H - C(0)]}{C(0)} \times 100$$

where ε′ (H) and C(0) is the value of the dielectric constant in the presence and absence of a magnetic field. The magneto capacitance response for the pure sample is positive while for the composites (x = 0.2) and (x = 0.4), it shows a negative and positive response on the application of magnetic field from 0 T to 0.8 T at 1 KHz. The findings from the variation of dielectric loss with frequency curve for $Mg_{1-x}Zn_xFe_2O_4$ nanocomposite indicate that the dielectric loss increases gradually with increasing frequency. This is due to the presence of electrical losses in the material due to the motion of charge carriers at the higher frequencies. The findings from the variation of dielectric constant as a function of magnetic field for $Mg_{1-x}Zn_xFe_2O_4$ nanocomposites reveals that the magneto-dielectric constant increases up to 2000 Oe, before decreasing for higher magnetic field strengths. This could be attributed to the presence of Zn^{2+} in the composite material.

VSM studies: Magnetic properties of $MgFe_2O_4$ nanoparticles and $Mg_{1-x}Zn_xFe_2O_4$ composites are studied using VSM

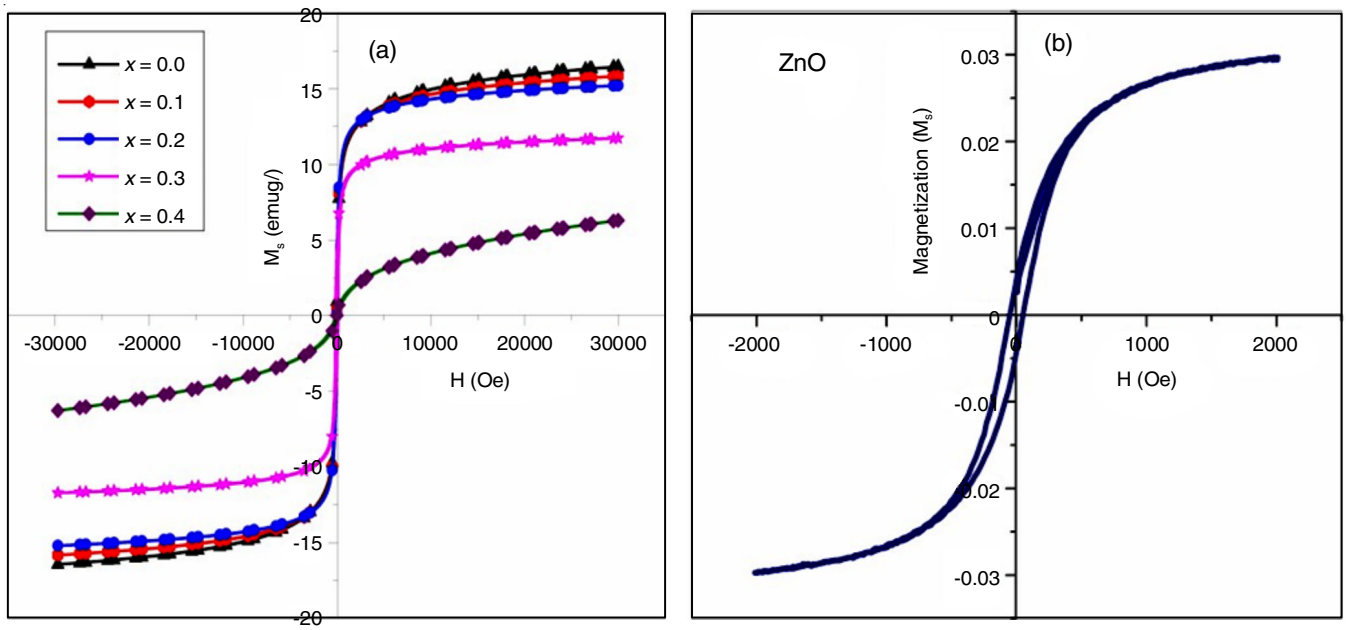

Fig. 8. Magnetization hysteresis loop for (a) ZnO, and (b) $Mg_{1-x}Zn_xFe_2O_4$ nanocomposites (x = 0.0, 0.1, 0.2, 0.3 and 0.4)

(vibrating sample magnetometer) analysis is shown in Fig. 8. This analysis measures the magnitude of magnetization of a material in response to an applied magnetic field [1,2]. It is used to study how the ferrimagnetic properties of these nanoparticles and composites are affected by the presence of zinc in $Mg_{1-x}Zn_xFe_2O_4$ composites. The results indicate that the introduction of zinc weakens the ferrimagnetic properties in $Mg_{1-x}Zn_xFe_2O_4$, which can be attributed to the decreased saturation magnetization and increased coercivity of the composites compared to pure $MgFe_2O_4$ nanoparticles (Fig. 9). Zinc excess or zinc deficiency incorporated Zn^{2+} mixed ferrite as observed because of coercivity is inversely proportional to the saturation magnetization $\{H_c = (K/M_s) \times 0.96\}$. From Table-2, $Mg_{1-x}Zn_xFe_2O_4$ nanocomposites shows that the crystallite size decreases from 40 to 19 nm and the lattice constant decreases from 8.432 Å to 8.399 Å. This indicates that the zinc substitution has a significant impact on the crystal structure of the composite. Additionally, the saturation magnetization decreases from 16 to 6 emu/g, while the coercivity increases from 19 G to 84 G [4,6,8]. Moreover, the magnetic moment decreases from 0.6639 to 0.2709 and the magnetic anisotropy constant increases from 316.666 to 962.500. The data suggests that zinc substitution has a strong influence on the ferrimagnetic properties of $Mg_{1-x}Zn_xFe_2O_4$ composites. The decrease in crystallite size and lattice constant indicate that zinc substitution has an effect on the crystal structure of the nanocomposite. The decrease in saturation magnetization and magnetic moment, combined with the increase in coercivity and magnetic anisotropy constant, suggest that zinc substitution increases the ferrimagnetic properties of the composite, leading to improve the performance in applications such as magnetic recording media and magnetic resonance imaging [14,19,25]. Because of zinc (Zn^{2+}) reduces the saturation magnetic moment, which is the magnitude of the magnetic dipole moment per unit volume. Zinc reduces the magneto-crystalline anisotropy, which is the degree of alignment of the magnetization within a material. Zinc also reduces the interaction and energy exchange between neighbouring atoms in a material through a process known as exchange coupling. Additionally, the higher coercivity leads to improved thermal stability and better magnetic stability. Additionally, improved energy exchange between metal ions can further enhance the magnetic properties of the nanoparticles, leading to improved performance in various applications [12-15,23-26].

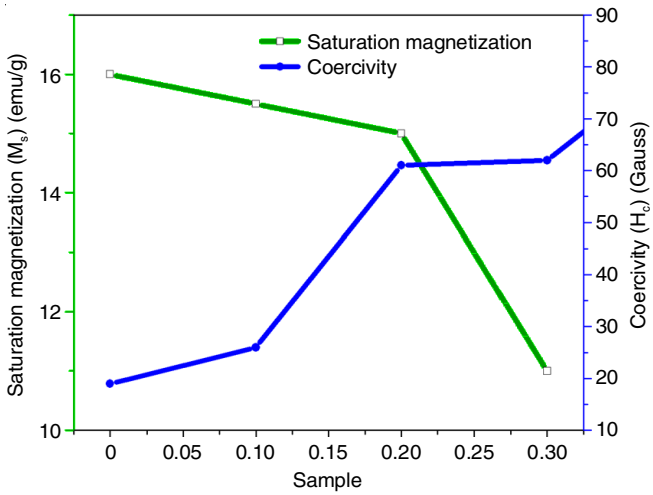

Fig. 9. Relation between magnetization and coercivity

TABLE-2
DATA ON MAGNETIC PARAMETERS OF $Mg_{1-x}Zn_xFe_2O_4$

Sample	Saturation magnetization (M_s) (emu/g)	Coercivity (H_c) (Gauss)	$\mu_B = M \times [M_s/5585]$	$K = (H_c \times M_s)/0.96$ erg/g
0.0	16.0	19	0.6639	316.666
0.1	15.5	26	0.6999	419.791
0.2	15.0	61	0.6774	953.125
0.3	11.0	62	0.4967	710.416
0.4	6.0	84	0.2709	962.500

TABLE-3
DATA ON ZONE OF INHIBITIONS (mm) OF $MgFe_2O_4$ AND $Mg_{0.6}Zn_{0.4}Fe_2O_4$

Microbial strains	0.0 @ Zone of inhibitions (mm)					0.4 @ Zone of inhibitions (mm)				
	Sample dose (µg/mL)			Std. (30 µL)	Control (30 µL)	Sample dose (µg/mL)			Std. (30 µL)	Control (30 µL)
	10	20	40			10	20	40		
Escherichia coli	4.20	10.05	13.55	14.75	Nil	4.55	10.35	13.95	14.65	Nil
Staphylococcus aureus	4.05	9.40	13.40	14.50	Nil	4.30	10.20	13.70	14.55	Nil

Antibacterial activity: The antibacterial activity of $MgFe_2O_4$ and $Mg_{0.6}Zn_{0.4}Fe_2O_4$ magnetic nanoparticles was tested against several pathogens using the well-diffusion method in nutrient agar medium. The antibacterial activity showed that these materials had an increased inhibition as the concentration, leading to the cessation of bacterial replication. It is believed that this antibacterial action is caused by positively charged ions, such as Mg^{2+}, Fe^{3+} and Zn^{2+} which interact with the damage bacterial membrane, impairing the electron transport chain and leading to cell death. These ROS can also cause DNA damage, enzyme protein peroxidation and membrane lipid peroxidation, which can further inhibit the functioning of the electron transport mechanism and lead to increased antibacterial activity (Table-3). The effects of substitution of Zn^{2+} ions in specific sites of magnesium ferrite were observed to be more effective in improving antibacterial activity than a small amount of Zn^{2+} exchanged in the material. Additionally, an increased surface area due to the small grain size was found to have a positive effect on the antibacterial activity. They can also interact with damage the bacterial membrane, impairing the electron transport chain and leading to cell death [2,30-35].

Conclusion

Zinc doped magnesium ferrite ($Mg_{1-x}Zn_xFe_2O_4$) nanocomposite was employed by the sol-gel method. The XRD analysis reveals that the crystallite size is between 19-40 nm and the lattice constant decreases (8.432-8.399 Å) with increasing Zn^{2+} content. The findings demonstrated that the presence of Zn^{2+} in the spinel structure affects its crystallite size and lattice constant. FTIR studies revealed that two major vibrational modes, namely the tetrahedral (446 cm^{-1}) and octahedral (584 cm^{-1}) sites, which indicated that the ferrite structure is composed of a combination of these two distinct sites.The dielectric constant results showed that the overall dielectric constant decreases as Zn^{2+} content increases. The value of the dielectric constant is highest at lower frequencies and gets reduced at higher frequencies. Vibrating sample magnetometer (VSM) and magnetization measurements were used to measure the saturation magnetization, coercivity and remanence of the composite material. The results showed that the saturation magnetization gradually decreases (16 to 6 emu/g) with increasing Zn^{2+} content. This decrease in magnetization may be attributed to the presence of non-magnetic Zn^{2+} embedded in the $MgFe_2O_4$ matrix. These findings provide insight into the magnetic behaviour of the material and could help in developing strategies to optimize its performance.The magneto dielectric constant analysis indicate that the composite material has a positive magneto-dielectric constant up to 2000 Oe, which then decreases for higher magnetic field strengths. Additionally, the material exhibits both a positive and a negative change in magneto-capacitance as a function of the applied magnetic field. The antibacterial activity results of this study have demonstrated that substitution of Zn^{2+} into magnesium ferrite can be an effective approach to improve antibacterial activity, likely due to the interaction between positively charged ions and ROS from nanoparticles damaging bacteria membrane and other components through positively charged ions and ROS generated by nanoparticles. Thus, the prepared zinc doped magnesium ferrite can be a promising candidate for a wide range of biomedical and technological applications.

ACKNOWLEDGEMENTS

The St. Joseph's College of Arts and Science (Autonomous) and Thiru.Vi.Ka. Government Arts and Science, provided the research lab and library facilities for which the authors are gratefully acknowledged.

CONFLICT OF INTEREST

The authors declare that there is no conflict of interests regarding the publication of this article.

REFERENCES

1. A. Vedrtnam, K. Kalauni, S. Dubey and A. Kumar, *AIMS Mater. Sci.*, **7**, 800 (2020); https://doi.org/10.3934/matersci.2020.6.800
2. A. Prakash, R. Sagayaraj, D. Jayarajan, S. Aravazhi, S. Sebastian, S. Sylvestre and C. Nyanga, *Chem. Africa*, **6**, 1269 (2023); https://doi.org/10.1007/s42250-022-00570-7
3. R. Sagayaraj, S. Aravazhi, P. Praveen and G. Chandrasekaran, *J. Mater. Sci. Mater. Electron.*, **29**, 2151 (2018); https://doi.org/10.1007/s10854-017-8127-4
4. R. Sagayaraj, S. Aravazhi and G. Chandrasekaran, *J. Supercond. Nov. Magn.*, **31**, 3379 (2018); https://doi.org/10.1007/s10948-018-4593-z
5. R. Sagayaraj, S. Aravazhi and G. Chandrasekaran, *J. Inorg. Organomet. Polym. Mater.*, **29**, 2252 (2019); https://doi.org/10.1007/s10904-019-01183-3
6. X. Zeng, Z. Hou, J. Ju, L. Gao, J. Zhang and Y. Peng, *Materials*, **15**, 2422 (2022); https://doi.org/10.3390/ma15072422
7. A. Manikandan, J. Judith Vijaya, M. Sundararajan, C. Meganathan, L. Kennedy and M. Bououdina, *Superlattices Microstruct.*, **64**, 118 (2013); https://doi.org/10.1016/j.spmi.2013.09.021
8. Z. Zhang, *Mater. Today Commun.*, **26**, 101734 (2021); https://doi.org/10.1016/j.mtcomm.2020.101734
9. S. Raghuvanshi, F. Mazaleyrat and S.N. Kane, *AIP Adv.*, **8**, 047804 (2018); https://doi.org/10.1063/1.4994015
10. M.A. Gabal and A.A. Al-Juaid, *J. Mater. Sci. Mater. Electron.*, **31**, 10055 (2020); https://doi.org/10.1007/s10854-020-03551-z
11. H. Saqib, S. Rahman, R. Susilo, B. Chen and N. Dai, *AIP Adv.*, **9**, 055306 (2019); https://doi.org/10.1063/1.5093221

12. H. Liu, A. Li, X. Ding, F. Yang and K. Sun, *Solid State Sci.*, **93**, 101 (2019); https://doi.org/10.1016/j.solidstatesciences.2019.05.005
13. P.Y. Reyes-Rodríguez, D.A. Cortés-Hernández, J.C. Escobedo-Bocardo, J.M. Almanza-Robles, H.J. Sánchez-Fuentes, A. Jasso-Terán, L.E. De León-Prado, J. Méndez-Nonell and G.F. Hurtado-López, *J. Magn. Magn. Mater.*, **427**, 268 (2017); https://doi.org/10.1016/j.jmmm.2016.10.078
14. S. Raghuvanshi, M. Satalkar, P. Tapkir, N. Ghodke and S.N. Kane, *J. Phys. Conf. Ser.*, **534**, 012031 (2014); https://doi.org/10.1088/1742-6596/534/1/012031
15. M.V. Nikolic, Z.Z. Vasiljevic, M.D. Lukovic, V.P. Pavlovic, J.B. Krstic, J. Vujancevic, N. Tadic, B. Vlahovic and V.B. Pavlovic, *Int. J. Appl. Ceram. Technol.*, **16**, 981 (2019); https://doi.org/10.1111/ijac.13190
16. R. Poongodi, S. Senguttuvan and R. Sagayaraj, *Asian J. Chem*., **35**, 1781 (2023); https://doi.org/10.14233/ajchem.2023.27807
17. J.P. Dhal, B.G. Mishra and G. Hota, *RSC Adv.*, **5**, 58072 (2015); https://doi.org/10.1039/C5RA05894E
18. V. Marghussian, Magnetic Properties of Nano-Glass Ceramics, In: Nano-Glass Ceramics Processing, Properties and Applications, William Andrew Applied Science Publishers, Chap. 4, pp. 181-223 (2015).
19. N. Sanpo, C.C. Berndt, C. Wen and J. Wang, *Acta Biomater.*, **9**, 5830 (2013); https://doi.org/10.1016/j.actbio.2012.10.037
20. R. Sagayaraj, *Int. Nano Lett.*, **12**, 345 (2022); https://doi.org/10.1007/s40089-022-00368-y
21. K.K. Kefeni, T.A.M. Msagati, T.T.I. Nkambule and B.B. Mamba, *Mater. Sci. Eng. C*, **107**, 110314 (2020); https://doi.org/10.1016/j.msec.2019.110314
22. M.I.A. Abdel Maksoud, M.M. Ghobashy, A.S. Kodous, R.A. Fahim, A.I. Osman, A.H. Al-Muhtaseb, D.W. Rooney, M.A. Mamdouh, N. Nady and A.H. Ashour, *Nanotechnol. Rev.*, **11**, 372 (2022); https://doi.org/10.1515/ntrev-2022-0027
23. Y. Wang, Y. Miao, G. Li, M. Su, X. Chen, H. Zhang, Y. Zhang, W. Jiao, Y. He, J. Yi, X. Liu and H. Fan, *Mater. Today Adv.*, **8**, 100119 (2020); https://doi.org/10.1016/j.mtadv.2020.100119
24. H. Malik, A. Mahmood, K. Mahmood, M.Y. Lodhi, M.F. Warsi, I. Shakir, H. Wahab, M. Asghar and M.A. Khan, *Ceram. Int.*, **40**, 9439 (2014); https://doi.org/10.1016/j.ceramint.2014.02.015
25. P. Manimuthu, N. Shanker, K.S. Kumar and C. Venkateswaran, *Physica B*, **448**, 354 (2014); https://doi.org/10.1016/j.physb.2014.03.051
26. M.A. Gabal, D.F. Katowah, M.A. Hussein, A.A. Al-Juaid, A. Awad, A.M. Abdel-Daiem, A. Saeed, M.M. Hessien and A.M. Asiri, *ACS Omega*, **6**, 22180 (2021); https://doi.org/10.1021/acsomega.1c02858
27. N.M. Sadik, A.A. Sattar, M.M. Rashad and H.M. Elsayed, *SN Appl. Sci.*, **2**, 620 (2020); https://doi.org/10.1007/s42452-020-2450-8
28. H. Singh and K.L. Yadav, *J. Am. Ceram. Soc.*, **98**, 574 (2015); https://doi.org/10.1111/jace.13316
29. Z. Zeng, H. Wu, C. Zhou, X. Qin, J. He, C. Ji, X. Deng, R. Gao, C. Fu, W. Cai, G. Chen, Z. Wang and X. Lei, *J. Asian Ceram. Soc.*, **8**, 1206 (2020); https://doi.org/10.1080/21870764.2020.1833416
30. S. Udhayan, R. Udayakumar, R. Sagayaraj and K. Gurusamy, *BioNanoSci.*, **11**, 703 (2021); https://doi.org/10.1007/s12668-021-00864-z
31. A. Prakash, R. Sagayaraj, D. Jayarajan, S. Aravazhi, G. Chandrasekaran and R. Nithya, *Asian J. Chem.*, **34**, 2288 (2022); https://doi.org/10.14233/ajchem.2022.23840
32. D. Jayarajan, R. Sagayaraj, S. Silvan, S. Sebastian, R. Nithya and S. Sujeetha, *Chem. Africa*, **6**, 1875 (2023); https://doi.org/10.1007/s42250-023-00615-5
33. R. Sagayaraj, T. Dhineshkumar, A. Prakash, S. Aravazhi, D. Jayarajan, G. Chandrasekaran and S. Sebastian, *Chem. Phys. Lett.*, **759**, 137944 (2020); https://doi.org/10.1016/j.cplett.2020.137944
34. O.A. Awoyinka, I.O. Balogun and A.A. Ogunnow, *J. Med. Plants Res.*, **1**, 63 (2007).
35. National Committee for Clinical Laboratory Standards (NCCLS), Performance Standards for Antimicrobial Disc Susceptibility Tests. PA: NCCLS Publications 25 (1993).